View metadata, citation and similar papers at core.ac.uk

brought to you by CORE

provided by Open Archive Toulouse Archive Ouverte

Open Archive Toulouse Archive Ouverte (OATAO)

OATAO is an open access repository that collects the work of Toulouse researchers and makes it freely available over the web where possible.

This is an author-deposited version published in: http://oatao.univ-toulouse.fr/
Eprints ID: 5585

To link to this article: DOI: 10.1021/jp210338t
URL: http://dx.doi.org/10.1021/jp210338t

To cite this version:

Duarte, Adriana P. and Gressier, Marie and Menu, Marie-Joëlle and Dexpert-Ghys, Jeannette and Caiut, José Mauricio A. and Ribeiro, Sidney J. L. *Structural and Luminescence Properties of Silica-Based Hybrids Containing New Silylated-Diketonato Europium(III) Complex.* (2012) Journal of Physical Chemistry C, vol. 2012 (n° 116). pp. 505-515. ISSN 1932-7447

Any correspondence concerning this service should be sent to the repository administrator: staff-oatao@listes.diff.inp-toulouse.fr

Structural and Luminescence Properties of Silica-Based Hybrids Containing New Silylated-Diketonato Europium(III) Complex

Adriana P. Duarte,[†,⊥] Marie Gressier,[†] Marie-Joëlle Menu,[*,†] Jeannette Dexpert-Ghys,[‡] José Maurício A. Caiut,[§] and Sidney J. L. Ribeiro[*,⊥]

[†]Centre Interuniversitaire de Recherche et d'Ingénierie des Matériaux, UPS-CNRS 5085, Université de Toulouse, 118 route de Narbonne, 31062 Toulouse Cedex 9, France

[‡]Centre d'Elaboration de Matériaux et d'Etudes Structurales, CNRS UPR 8011, 21 rue J. Marvig, B.P. 94347, 31055, Toulouse Cedex 4, France

[§]Department of Chemistry, University of São Paulo, FFCLRP, Ribeirão Preto-SP, Brazil

[⊥]Institute of Chemistry, São Paulo State University, UNESP, CP355-Araraquara-SP, 14801-970 Brazil

ABSTRACT: A new betadiketonate ligand displaying a trimethoxysilyl group as grafting function and a diketone moiety as complexing site (TTA-Si = 4,4,4-trifluoro-2-(3-trimethoxysilyl)propyl)-1-3-butanedione $(C_4H_3S)COCH[(CH_2)_3Si(OCH_3)_3]COCF_3$) and its highly luminescent europium(III) complex $[Eu(TTA\text{-}Si)_3]$ have been synthesized and fully characterized. Luminescent silica-based hybrids have been prepared as well with this new complex grafted on the surface of dense silica nanoparticles (28 ± 3 nm) or on mesoporous silica particles. The covalent bonding of $Eu(TTA\text{-}Si)_3$ inside the core of uniform silica nanoparticles (40 ± 5 nm) was also achieved. Luminescence properties are discussed in relation to the europium chemical environment involved in each of the three hybrids. The general methodology proposed allowed high grafting ratios and overcame chelate release and tendency to agglomeration, and it could be applied to any silica matrix (in the core or at the surface, nanosized or not, dense or mesoporous) and therefore numerous applications such as luminescent markers and luminophors could be foreseen.

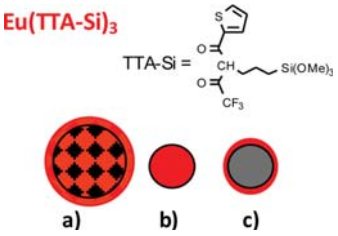

1. INTRODUCTION

Lanthanide complexes take the part of an important class of compounds for the development of advanced luminescent materials with applications in optoelectronics, imaging, markers, OLEDs, and fluorescent lamps.[1−7] They are strong light emitters despite the well-known low absorption coefficients for UV−visible light due to the forbidden nature of 4f−4f electronic transitions. Fortunately, as well established in the past decades, the low absorption for exciting photons may be circumvented by using strong UV absorbing particular ligands that leads to relatively intense visible emission bands under UV excitation due to the efficient intramolecular energy transfer from the ligands to the metal ion in the so-called "antenna effect".[1−6] The list of potential ligands is copious and many reviews devoted to lanthanide-related properties were reported in the last years.[4−6] To explore the potential of the lanthanides complexes for a number of applications, it is useful to load them in an inert host matrix. The sol−gel process is a well-known process for preparing organic/inorganic hybrid materials which properties (mechanical, thermal, physical, and chemical) that can be further tailored by modifying the processing conditions. Therefore, microstructure, shape, and degree of connection of the two networks have to be controlled.

In parallel, silica-based materials are well established in many applications fields. In bioanalysis applications, for example, polystyrene nanoparticles doped with fluorescent chelates were first explored.[8] However, they suffer from drawbacks such as risk of chelate release, tendency to agglomerate, and difficulty to separate from solution. As an alternative, functionalized silica nanoparticles have been developed mainly because of interesting properties such as inherent hydrophilicity, flexible surface modification, and ready separation from solution.

Generally, the methods reported to elaborate lanthanide-containing organic/inorganic materials involve first the incorporation of organic ligands into the inorganic matrix by low-temperature soft-chemistry processes. Organosilane species have been used as coupling agents to induce covalent bond between the metal ion and the matrix in a conventional sol−gel procedure. Thermal stability, photophysical properties, and the processing facility of the hybrids were observed to be improved compared to the lanthanide complexes. This general route is described in Scheme 1a where sol−gel glasses[9−13] thin films[14] containing europium(III) or another Ln(III) as luminescent center have been reported. Luminescent materials with europium complex anchored in aminoalkoxysilane-modified mesoporous silica[15,16] have also been described.

In other works, complexation reactions of organically modified silica surfaces with europium salts or chelates, as described in

Scheme 1. Representation of Different Methodologies Used To Obtain Luminescent Silica-Based Materials Containing Covalently Bonded Europium(III) Complexes[a]

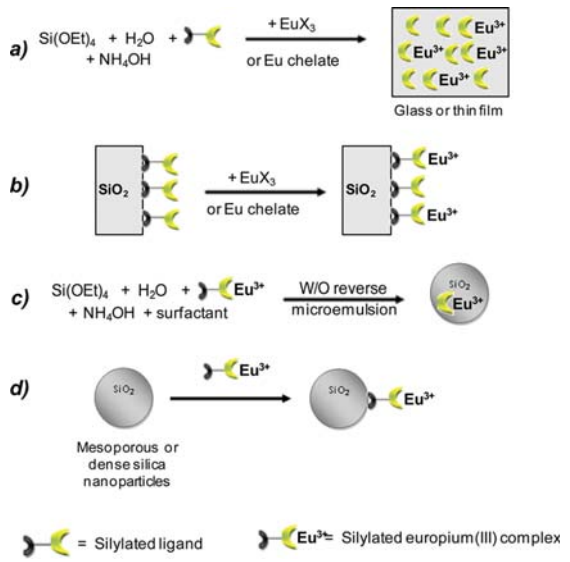

[a] (a) Introduction of Eu^{3+} salt or chelate in a one-pot synthesis of glasses or thin films. (b) Eu^{3+} complexation on organically modified silica matrix. (c) Incorporation of silylated Eu^{3+}complex in a Stober-type reaction using W/O reverse microemulsion system. (d) Grafting of silylated Eu^{3+}complex on the surface of mesoporous or dense silica nanoparticles.

Scheme 1b, have been followed for different silica substrates: mesoporous silica,[17−20] micronic silica particles,[21] or functionalized silica surface of silicon wafer.[22]

Interest in organosilane reagents lies in the possibility to obtain organically modified silica-coated materials and nanomaterials for bioanalysis. When organosilane contains donor heteroatom, silylated complexes can be designed in order to functionalize in a homogeneous way the core (Scheme 1c) or the surface (Scheme 1d) of nanosized silica.

Very few silylated lanthanide complexes have been isolated and fully characterized. Binnemans and Driesen reported sol−gel glasses[10] and thin films[14] bearing a homogeneous distribution of covalently linked lanthanides complexes using substituted phenanthroline ligands as anchoring ligands. Silylated ligands prevent the nonhomogeneous embedding of the luminescent complex in the host matrix which could be responsible of the decrease of the luminescence intensity. Distinctive examples of organosilanes exhibiting bidentate nitrogen ligands as complexing site and exploited in the different methodologies presented herein are given in Scheme 2.

Monosilylated derivatives such as pyridylpyrazolyl, Pypy-Si, have been used to functionalize MCM41 mesoporous silica matrix in the route b (Scheme 1) by Carlos and colleagues,[20] whereas the phenanthroline molecule, Phen-Si, was grafted on wafer silica surface[22] involving the same route b (Scheme 1). In both cases, the silylation is realized by reacting isocyanatopropyltrialkoxysilane (IPTES, $NCO(CH_2)_3Si(OEt)_3$) with aminated pyrazolyl or phenanthroline frameworks. When 2 equiv of IPTES was employed, disilylated ligand is isolated and generally used to ascertain metal complex anchoring in sol−gel glasses or thin film processes as reported by Zhang.[9] Such disilylated

Scheme 2. Silylated Bidentate Ligands (Pypy-Si,[20] Phen-Si,[22] Phen-Si_2,[9] and TTA-Si_2[26]) and Europium(III) Complexes

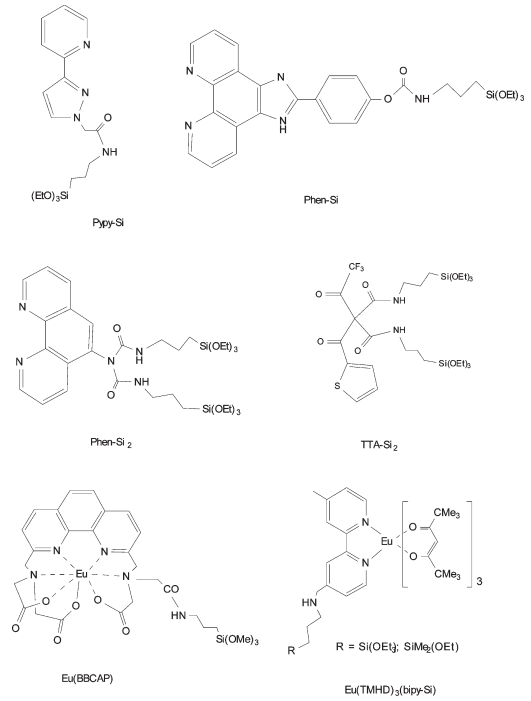

phenanthroline derivative is illustrated in Scheme 2 with the Phen-Si_2 molecule.

Another benefit related to the silylated complexes is to prevent dye release when this latter is incorporated in the core of the silica nanoparticles as reported by Li et al.[23] with dual-lanthanide-chelated silica nanoparticles as labels in bioanalysis. In this later study, a phenanthroline molecule has been chemically modified by reaction with aminopropyltriethoxysilane in order to introduce anchoring group to the ligand. Both terbium and europium(III) complexes (Ln(BBCAP), Scheme 2) are previously formed and then covalently incorporated in 40 nm silica nanoparticles using a ternary water in oil microemulsion illustrating the route c presented in Scheme 1. Because nanoparticles contain thousands of fluorescent lanthanide chelates, ultrasensitive time-resolved immunofluorometric assay can be undertaken using these nanohybrids. This example is totally in agreement with our previous work which illustrated well the last methodology reported to obtain luminescent silica-based nanomaterials (d, Scheme 1). We have shown that it is possible to functionalize the silica surface of nanosized particles with silylated dipyridine europium complexes,[24] ($Eu(TMHD)_3$(bipy-Si) with bipy-Si = $(EtO)_3Si(CH_2)_3NHCH_2$-bipy or $(EtO)(CH_3)_2Si(CH_2)_3NHCH_2$-bipy, Scheme 2). Moreover, monolayer of europium complex is ascertained when monoethoxysilyldipyridine ligand is chosen as anchoring group.[25]

Diketone ligands such as dibenzoylmethane[17](DBM), acac,[17,26] or 2-thenoyltrifluoroacetone[26] (TTA) have been used respectively by Serra and Yan to synthesize polymeric molecular-based lanthanides hybrids. In the last case, the hybrid polymer reported contains disilylated TTA molecule (TTA-Si_2, Scheme 2) obtained by reaction of 2 equiv of IPTES with 1 equiv of TTA. The utilization of the TTA-Si_2 ligand and in situ formation of the europium complex both prevent the clustering and/or leaching

Scheme 3. Silylated TTA Ligand, TTA-Si, and Related Europium(III) Complex, Eu(TTA-Si)$_3$

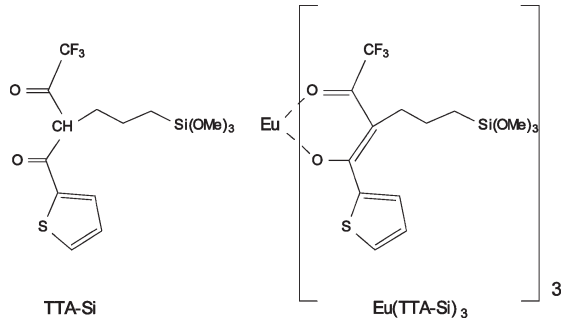

of the emitting center and ascertains homogeneous dispersion of the two phases.

We focused our work on silica particles which constitute good platforms for the development of efficient light emitters for lighting and luminescent markers or probes. Spherical silica particles may be prepared with controlled size, from a few nanometers to a few micrometers, by well-defined sol−gel methods. Due to the possibility of incorporation of active species (luminescent or magnetic), silica nanoparticles may be considered as nanobuilding blocks for which the surface has to be tailored aiming multifunctionality. In this way, silylated complexes allow the functionalization of the core of the particles by covalent interactions. They also give the possibility to be covalently grafted on any silica surfaces. The alternative and original route proposed by us involves previous preparation of organosilylated lanthanide complexes which were afterward grafted on a specific substrate including nanosized matrix. The advantages are obvious since one can previously design the substrate with any size, morphology, porosity, and other adjusted characteristics with a covalent bonding poststep of the lanthanide luminescent species. It is what we undertake in this work, taking advantage of one of the best known β-diketone ligands to synthesize highly luminescent europium complexes. We have chosen to synthesize europium complex containing monosilylated 2-thenoyltrifluorodiketone (TTA-Si, Scheme 3) in order to have the best control of the hydrolysis and condensation reactions involved in the grafting and incorporation processes. The so-obtained efficient light-emitting Eu^{3+} complex, Eu(TTA-Si)$_3$ (Scheme 3) has been loaded on different silica-based substrates involving the methodologies c and d presented in Scheme 1. Results are reported here for grafted commercial dense silica nanoparticles, and mesoporous spherical silica particles obtained by spray pyrolysis.[27] Successful incorporation of the new Eu(TTA-Si)$_3$ complex in silica nanoparticles by the so-called Stober methodology c (Scheme 1) using a water in oil reverse microemulsion system is also described. Luminescence properties are examined and discussed with respect to an eventual application of these hybrids as luminescent biolabels.

2. EXPERIMENTAL SECTION

2.1. Materials. 3-Chloropropyltrimethoxysilane, Triton X-100, and 1-octanol were purchased from Acros, thenoyltrifluoroacetone (TTA), sodium hydride, europium chloride hexahydrate, gadolinium chloride hexahydrate from Aldrich, tetraethoxysilane (TEOS) from ABCR, and cyclohexane from SDS. These regents were used as received. Ludox AS40, obtained from Aldrich, was used as starting silica material. It contains 40 wt % SiO_2, with an average particle size of 24 ± 2 nm, and the specific surface area determined from BET is 138 m^2/g. Spherical mesoporous SiO_2 particles were obtained by spray pyrolysis methodology as described in a previous work,[27] using cetyltrimethylammonium bromide (CTAB) as structure-directing agent. The samples are polydispersed (50 nm−2.5 μm) with an average size of 600 ± 300 nm. Specific surface area value (BET) is 940 m^2/g. Tetrahydrofuran, dichloromethane, methanol, diethyl ether, and ethanol were purified by distillation in an inert atmosphere before use. All manipulations concerning the preparation of ligand and complexes were performed in an inert atmosphere using the Schlenk tube technique. Aqueous solutions were prepared with ultrapure water (18.2 MΩ/cm) obtained from a Millipore Milli-Q water purification system.

2.2. Characterization Methods. FTIR and DRIFT spectra were obtained in the spectral range from 4000 to 400 cm^{-1} with a Bruker Vector 22 (KBr dispersion) and a Perkin-Elmer 1760 (DRIFT, DTGS detector) spectrometers, respectively. ^1H and ^{13}C $\{^1H\}$ NMR spectra in $CDCl_3$ were measured using a Bruker Avance 300 (300.180 and 75.468 MHz for ^1H and ^{13}C, respectively) for the characterization of the TTA-Si ligand. Mass spectra were recorded by FAB using a Nermag R10-10 spectrometer or a TSQ 7000 Thermo-Quest Spectrometer. UV−vis spectra were recorded using a Varian UV−visible Cary 1E spectrometer in the range 900−200 nm. Elemental analyses of C, H, and S were performed on a Carlo Erba instrument (EA 1110). Luminescence spectra were measured at room temperature using a Jobin-Yvon Model Fluorolog FL3-22 spectrometer equipped with a R928 Hamamatsu photomultiplier and a 450 W Xe excitation lamp. Excitation and emission spectra were recorded under CW excitation and were corrected with respect to the Xe Lamp intensity and spectrometer response. Measurements of emission decay were performed with the same equipment by using a pulsed Xe (3 μs bandwidth) source. Particle shape and size were examined via TEM, using a Philips Model CM20 FEG microscope. A drop of sol was diluted in ethanol.

2.3. Synthesis. *2.3.1. TTA-Si:4,4,4-Trifluoro-2-(3-(trimethoxysilyl)-propyl)-1-(2-thienyl)-1,3-butanedione, $(C_4H_3S)COCH[(CH_2)_3Si(OCH_3)_3]$-$COCF_3$.* Two mmol (444.36 mg) of 2-thenoyltrifluoroacetone (TTA) was added to 20 mL of anhydrous tetrahydrofuran under stirring, 2 mmol (48 mg) of sodium hydride was added and the mixture was refluxed for 90 min, and then 2 mmol (371 μL) of 3-chloropropyltrimethoxysilane was added dropwise under stirring and reflux was maintained under nitrogen atmosphere for 18 h. The solvent was evaporated; the product was dissolved in diethyl ether and filtered. The resulting solution was evaporated, leading to the solid compound TTA-Si ($C_{14}H_{19}F_3O_5SSi$, MW: 384.44). Yield: 87%. Elemental analysis for $C_{14}H_{19}F_3O_5SSi$, %, found (calcd): C 43.62 (43.69), H 4.83 (4.98), S 8.27 (8.32). FTIR (KBr, cm^{-1}): 3104 ν_{as}(C−H); 2995 $\nu_{as}(CH_2,CH_3)$; 2877 $\nu_s(CH_2,CH_3)$; 1620 ν(C--O); 1535 and 1516 ν(C--O, C--C); 1501, 1481, 1415, and 1355 ν(C═C,C═S thienyl); 1280 $\nu(CF_3)$; 1244 ν(C−Si); 1191 and 1180 ρ(Si−O−CH_3); 1149 ν(Si−O); 1059 δ(O−CH_3); 933 δ(Si−O−C); 861 $\delta(CH_3)$; 785 δ(CH thienyl); 712 and 702 $\delta(CF_3)$. ^1H NMR (δ ppm, $CDCl_3$): 0.78 (m, 2H, CH_2 (11)); 1.89 (m, 2H, CH_2 (10)); 3.40 (m, 2H, CH_2 (9)); 3.68 (s, 9H, CH_3 (12)); 6.22 (t, 1H, CH (6)); 7.06 (d, 1H, CH (2)); 7.55 (d, 1H, CH (1)); 7.67 (d, 1H, CH (3)). $^{13}C\{^1H\}$ NMR (δ ppm, $CDCl_3$): 5.30 (s, CH_2, (10)); 23.83 (s, CH_2, (11)); 44.00 (s, CH_2, (9)); 49.61 (s, CH_2, (12)); 90.24 (s, CH, (6)); 117.19 (q, ^{1}JC-F = 293 Hz,

CF_3, (8)); 127.29 (s, CH thienyl, (3)); 129.64 (s, CH thienyl, (2)); 132.50 (s, CH thienyl, (1)); 148.05 (s, C thienyl (4)); 169.13 (q, ^{2}JC-F = 31.9 Hz, CO, (7)); 181.89 (s, CO, (5)). SM (FAB): m/z = 385 [M^+]; UV (acetonitrile): 257 nm (ε = 14 050 L mol^{-1} cm^{-1}), 338 nm (ε = 32 800 L mol^{-1} cm^{-1}).

2.3.2. Eu(TTA-Si)$_3$. Six mmol (2.30 g) of the TTA-Si and 2 mmol (0.732 g) of europium chloride hexahydrate were added to 20 mL of anhydrous ethanol. The reaction mixture was kept under nitrogen atmosphere and stirred for 18 h. Solvent was evaporated, and the resulting powder was washed with pentane and diethyl ether, and dried under vacuum. The Eu(TTA-Si)$_3$ complex ($EuC_{42}H_{54}F_9O_{15}S_3Si_3$, MW 1302.27) was obtained as a brownish powder. Yield: 76%. Elemental analysis for $EuC_{42}H_{54}O_{15}F_9S_3Si_3$, 76%, found (calcd): C 38.20 (38.76), H 3.98 (4.18), S 7.29 (7.38). FTIR (KBr, cm^{-1}): 3109 ν_{as}(C−H); 2977 ν_{as}(CH_2,CH_3); 2875 ν_s(CH_2,CH_3); 1627 ν(C⁻⁻O); 1533 (br) and 1520 (br) ν(C⁻⁻O, C⁻⁻C); 1505 (sh), 1485 (sh), 1414 and 1355 ν(C═C, C═S thienyl); 1285 ν(CF_3); 1241 ν(C−Si); 1184 ρ(Si−O−CH_3); 1144 ν(Si−O); 1058 δ(O−CH_3); 932 δ(Si−O−C); 860 δ(CH_3); 783 δ(CH thienyl); 723 δ(CF_3). Mass spectrum (FAB): m/z 1300 [M^+]; UV (acetonitrile) 276 nm (ε = 33 400 L mol^{-1} cm^{-1}), 341 nm (ε = 41 350 L mol^{-1} cm^{-1}).

2.3.3. Gd(TTA-Si)$_3$. This complex was obtained by the procedure described for Eu(TTA-Si)$_3$ and starting with 6 mmol (2.30 g) of the TTA-Si and 2 mmol (0.742 g) of gadolinium chloride hexahydrate. The Ga(TTA-Si)$_3$ complex ($GdC_{42}H_{54}F_9O_{15}S_3Si_3$, MW 1307.56) was obtained as a yellow powder. Yield: 78%. Elemental analysis ($GdC_{42}H_{54}O_{15}F_9S_3Si_3$), %, found (calcd): C 37.70 (38.55), H 3.87 (4.16), S 7.32 (7.34). FTIR (KBr, cm^{-1}): 3109 ν_{as}(C−H); 2957 ν_{as}(CH_2,CH_3); 2878 ν_s(CH_2,CH_3); 1627 ν(C⁻⁻O); 1537 (br) and 1517 (br) ν(C⁻⁻O, C⁻⁻C); 1500 (sh), 1479 (sh), 1415 and 1353 ν(C═C,C═S thienyl); 1280 ν(CF_3); 1243 ν(C−Si); 1191 ρ(Si−O−CH_3); 1133 ν(Si−O); 1057 δ-(O−CH_3); 933 δ(Si−O−C); 860 δ(CH_3); 786 δ(CH thienyl); 705 δ(CF_3). Mass spectrum (FAB): m/z 1308 [M^+]; UV (acetonitrile): 286 nm (ε = 24 150 L mol^{-1} cm^{-1}), 339 nm (ε = 52 750 L mol^{-1}cm^{-1}).

2.3.4. Luminescent Hybrids. Two different procedures were used as schematically shown in Scheme 1. Using the procedure d, the complex was grafted at the particle surface (Ludox AS40 and mesoporous silica) whereas in procedure c the complex was incorporated during the silica particles preparation by a modified Stober synthesis using water in oil reverse microemulsion methodology. The hybrids are denoted SiO_2*meso*-Eu(TTA-Si)$_3$, SiO_2−Eu(TTA-Si)$_3$, and SiO_2@Eu(TTA-Si)$_3$ for different silica matrix, i.e., mesoporous silica, Ludox AS40, and incorporating process, respectively.

2.3.4.1. SiO_2-meso-Eu(TTA-Si)$_3$ and SiO_2−Eu(TTA-Si)$_3$. Ludox silica sol (500 mg) or mesoporous silica (200 mg heat-treated at 200 °C for 6 h) was suspended in ethanol (10 mL) and reacted with 0.16 mmol (208 mg) Eu(TTA-Si)$_3$. The mixtures were stirred for 72 h at 295 K in air atmosphere. The resulting suspensions were dialyzed for 72 h, and the solids were isolated by centrifugation at 15 000 rpm for 15 min. The obtained solids were washed with ethanol, dichloromethane, and diethyl ether and then dried in vacuum for 2 h. Elemental analysis: SiO_2−Eu-(TTA-Si)$_3$, %, found (calcd): R = 0.21 mmol/g, C 7.85 (10.58), H 1.58 (1.13), S 2.02 (2.01) ; SiO_2-*meso*-Eu(TTA-Si)$_3$, %, found (calcd): R = 0.41 mmol/g, C 18.48 (20.66), H 2.07 (2.21), S 3.93 (3.93). DRIFT for both sample (KBr, cm^{-1}): 1630 υ(C═O); 1414 weak υ(C═C + C═S); 1230−1050 υ(Si−C) + υ(Si−O) + δ(Si−O−C); 950 δ(Si−O) and 800 δ(Si−O).

2.3.4.2. SiO_2@Eu(TTA-Si)$_3$. A solution of 20 mg of Eu(TTA-Si)$_3$ dissolved in 2 mL of octanol was added to a W/O microemulsion which was prepared by mixing 4.6 mL of TritonX-100, 20 mL of cyclohexane, and 3 mL of *n*-octanol. Afterward, 266 μL of TEOS and 160 μL of NH_4OH were added. The reaction was kept under stirring by 24 h followed by addition of acetone in order to break the microemulsion and recover the particles. The particles were washed with water, ethanol, and diethyl ether and then dried in vacuum for 2 h.

Elemental analysis: SiO_2@Eu(TTA-Si)$_3$, %, found (calcd): R = 0.12 mmol/g, C 4.68 (6.05), H 1.48 (0.64), S 1.14 (1.14). DRIFT (KBr, cm^{-1}): 2980 ν_{as}(CH_2,CH_3); 2878 ν_s(CH_2,CH_3) 1630 υ(C═O); 1414 weak υ(C═C + C═S); 1230−1050 υ(Si−C)+ υ(Si−O)+δ(Si−O−C); 950 δ(Si−O) and 800 δ(Si−O).

3. RESULTS AND DISCUSSION

3.1. Characterization and Luminescence Properties of Eu(TTA-Si)$_3$ Complex. Considering the interesting energy transfer which occurs from the TTA ligand to the electronic level of europium, we have chosen to synthesize a new ligand derived from TTA molecule bearing an anchoring function, i.e., trialkoxysilyl group, to covalently bond europium complexes to silica-based materials. According to the literature discussed earlier, we have introduced only one trialkoxysilyl group on the diketone moiety in order to minimize the possibility of hydrolysis and condensation of the ligand and then of the expected complexes. Moreover, we preferred chloropropyltrimethoxysilane $(MeO)_3Si(CH_2)_3Cl$ (CPTMS) as coupling agent to give rise to alkylated silane instead of isocyanatopropyltrimethoxysilane (ICPTES), which gives rise to the amide derivative; indeed, alkylated derivatives are known to be more stable to drastic pH conditions than amides. So monosilylation was undertaken as described in Scheme 4 (reactions i and ii) using only 1 equiv of sodium hydride and CPTMS. In controlled experimental conditions (dry organic solvent), the organosilyl-β-diketone ligand (TTA-Si) was synthesized in good yield (87%). The silylated ligand obtained by the α-carbon substitution from β-diketone ligands was corroborated by the ^{1}H and ^{13}C {^{1}H} NMR spectra. Assignments were done according to the atom numbering gave in Scheme 4. In ^{1}H NMR, while signals corresponding to the three hydrogen atoms of the thenoyl cycle are relatively unchanged, the presence of the three signals at 0.78, 1.89, and 3.40 ppm corresponding to the propyl chain confirms the success of the silylation reaction. The hydrogen atom signal in the α-position of diketone is a triplet observed at 6.22 ppm as expected for such methylene group in agreement with the monosilylation.

Moreover, integration of the signals confirms also that the silylated ligand is not hydrolyzed since the signal at 3.68 ppm assigned to the methoxy hydrogen atoms integrates for nine hydrogen atoms. ^{13}C {^{1}H} results confirmed the structure of the ligand exhibiting one signal for each magnetically inequivalent carbon atom and the assignment of the 12 signals is done in the Experimental Section. FTIR data support the organosilyl-β-diketonate ligand synthesis and the stability against the self-polymerization process by the observation of the vibration bands of the Si−O−CH_3 group at 1191 and 1180 cm^{-1} for the rocking vibration and 1059 cm^{-1} for the deformation. Silyl group was characterized by three other bands at 1244, 1149, and 933 cm^{-1} for ν(Si−C), ν(Si−O), and δ(Si−O−C), respectively. Additional bands from TTA moiety were observed at 1501, 1481,

Scheme 4. Synthesis Processes of the Silylated Ligand TTA-Si (i and ii) and the Corresponding Complex, Eu(TTA-Si)$_3$ (iii)[a]

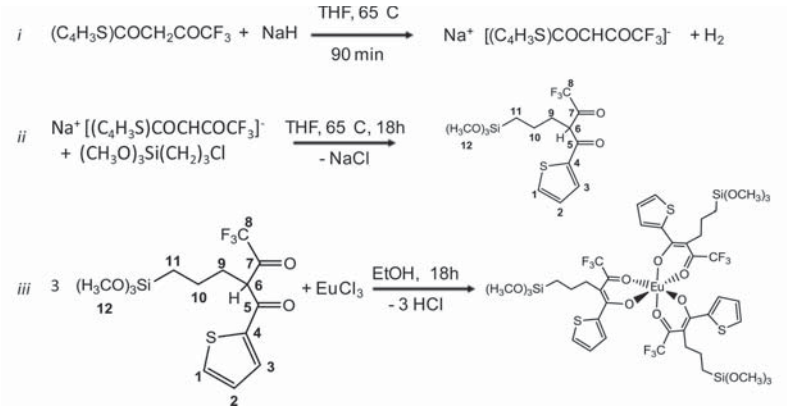

[a] Atom numbering in TTA-Si (ii) is related to assignments of NMR data.

1415, and 1355 cm^{-1} as fine and intense bands assigned to ν(C═C,C═S) in the thienyl heterocycle. Characteristic stretching vibration of the enol tautomer form of β-diketonate appeared at 1620 ν(C¯O), 1535 and 1516 ν(C¯O, C¯C) fine and intense bands. CF_3 characteristic vibrations are observed at 1280 cm^{-1}-($\nu(CF_3)$) and 704 and 712 cm^{-1}($\delta(CF_3)$). The molecular structure is definitively ascertained by mass spectrometry since FAB spectrum shows the molecular peak at m/z = 385 for [M$^+$] species.

Three equivalents of TTA-Si were reacted with europium chloride hexahydrate at room temperature in dry ethanol to give the Eu(TTA-Si)$_3$ complex as a brownish solid obtained after washings (reaction iii in Scheme 4). In the presence of europium chloride the deprotonation reaction of TTA-Si does not require addition of a base but the complexation reaction is maintained for 18 h. Elemental analysis is in agreement with the proposed formula. The presence of the TTA-Si ligand is confirmed by IR analysis with the stretching vibrations of the carbonyl functions at 1627 and 1533 cm^{-1} and those of the thienyl ring at 1505, 1485, 1414, and 1355 cm^{-1}. However, the complexation of TTA-Si modifies the shape of the 1530−1480 cm^{-1} region; indeed the two fine and intense bands at 1501 and 1481 cm^{-1} observed in the ligand spectrum appears as two shoulders (1505 and 1485 cm^{-1}) in the complex spectrum. The complexation reaction conditions exclude hydrolysis and self-polymerization of methoxysilyl groups since the vibration bands at 1184 and 1059 cm^{-1} indicate the presence of the Si−O−CH_3 group. Carbonyl, propylsilyl, and CF_3 vibration bands are very slightly affected by the complexation process. Well-characterized X-ray diffraction patterns could not be obtained for the powders and all attempts to obtain monocrystals were unsuccessful. Nevertheless, the molecular structure is ascertained by mass spectrometry that shows a major molecular peak at m/z = 1300 corresponding to [M$^+$], the isotopic pattern being in agreement with the proposed formula.

Figure 1 shows absorption spectra obtained for TTA-Si (spectrum a), Eu(TTA)$_3$, 2H_2O (spectrum b) for comparison purpose, and Eu(TTA-Si)$_3$ complex (spectrum c) (solutions at 2.5 × 10^{-5} mol/L in acetonitrile). The TTA-Si absorption was characterized by a strong and broad absorption centered at 338 nm, and this one was shifted at 341 nm for the Eu(TTA-Si)$_3$ complex. At shorter wavelengths, a well-defined band is observed at 257 nm in TTA-Si. The spectrum of Eu(TTA)$_3$(H_2O)$_2$

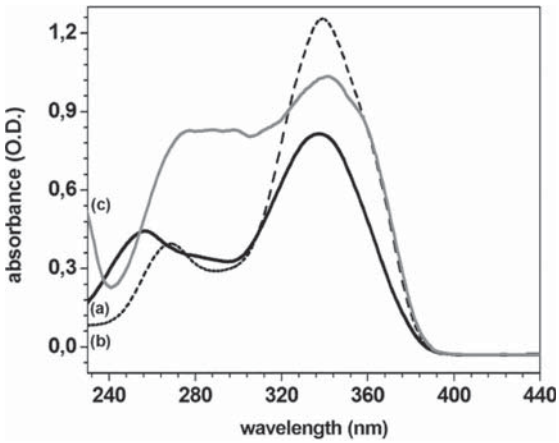

Figure 1. Absorption spectra (2.5 × 10^{-5} mol/L acetonitrile) of (a, black) TTA-Si; (b, dash) Eu(TTA)$_3$·2H_2O; and (c, gray) Eu(TTA-Si)$_3$.

in acetonitrile, also shown in Figure 1 (spectrum b), displays two relatively resolved bands at 269 and 339 nm which have been assigned to singlet-to-singlet transitions in the TTA ligands.[28,29] The same attribution is done here for the silylated ligand and its europium complex. In the 280−300 nm range, the additional absorption in Eu(TTA-Si)$_3$ compared with TTA-Si is tentatively assigned to the O−Eu charge-transfer state.

Figure 2 gathers the luminescence excitation and emission spectra recorded for the solid complex and an acetonitrile solution (2.5 × 10^{-6} mol/L). Spectra obtained for the solid Eu(TTA)$_3$(H_2O)$_2$ are also shown for comparison purposes. The broad and intense excitation observed at wavelengths below 400 nm is characteristic of the "antenna effect", i.e., the absorption in the ligand and the energy transfer to the Eu^{3+} emitting levels. The broad excitation band recorded for the solution reproduces essentially the absorption spectrum of Figure 1c; the band centered at 338 nm, being attributed to singlet-to-singlet transition in the TTA ligand,[28] has two maxima at 326 and 352 nm. The intra-4f^6 narrow excitation lines at around 464 nm ($^7F_{0,1} \rightarrow {}^5D_2$) are observed for the solid complex, but are hardly observed in the solution. Details on the singlet and triplet states of TTA-Si ligand have been obtained from the luminescence spectra of the gadolinium complex Gd(TTA-Si)$_3$, recorded

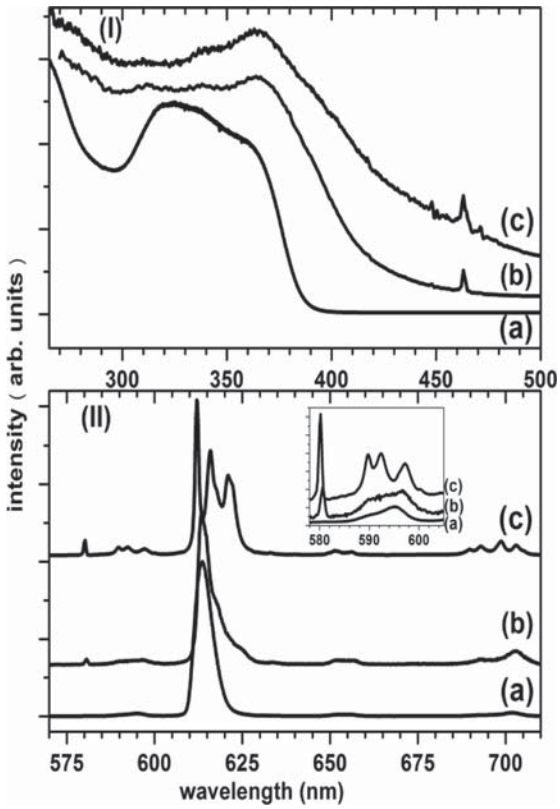

Figure 2. (I) Excitation spectra ($\lambda_{emission}$ at 612 nm) and (II) emission spectra ($\lambda_{excitation}$ at 365 nm) for the different samples, at 298 K: (a) Eu(TTA-Si)$_3$ acetonitrile solution (2.5×10^{-6} mol/L); (b) Eu(TTA-Si)$_3$ solid sample; and (c) Eu(TTA)$_3 \cdot (H_2O)_2$ solid sample. Inset: 575−605 nm enlargement, $^5D_0 \rightarrow {}^7F_0$ and $^5D_0 \rightarrow {}^7F_1$ transitions.

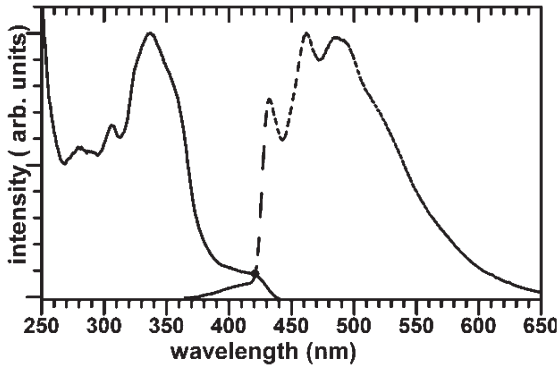

Figure 3. Excitation spectrum ($\lambda_{emission}$ at 462 nm, full line) and emission spectrum ($\lambda_{excitation}$ at 336 nm, dashed line) for the Gd-(TTA-Si)$_3$ solid sample, at 77 K.

at liquid nitrogen temperature. The excitation and emission spectra are shown in Figure 3. The first excited electronic levels of Gd^{3+} being at higher energies (^5I_J at around 36 900 cm^{-1}), there is no gadolinium emission in the visible range and all the luminescence observed is due to the ligand part of the complex. The emission observed between 400 and 600 nm can be in this way assigned to triplet to ground-state transition (~480 nm to ~20 830 cm^{-1}). There are three rather well-defined bands at 430, 460, and 480 nm, which could be due to emissions from different electronic triplet states, but could also be vibronic replicas usually observed superposed to these triplet emission bands.[30] As a matter of fact, all these features appear at energies higher than the one of Eu^{3+} $^5D_0$ state so that the energy transfer from the triplet states to $^5D_0$ is favorable while back-transfer would be less probable. The fact that the broad phosphorescence from ligand triplet states is not observed in the Eu(TTA-Si)$_3$ complex indeed suggests an efficient ligand to Eu^{3+} energy transfer.

Emission spectra of the europium complexes are displayed in Figure 2(II). The intra-4f^6 Eu^{3+} transitions from the $^5D_0$ to ^7F_J levels are easily identified. For the Eu(TTA-Si)$_3$ solid complex, the following emission lines are seen: $^5D_0 \rightarrow {}^7F_0$ (580.6 nm), $^5D_0 \rightarrow {}^7F_1$ (592 and 596.8 nm), $^5D_0 \rightarrow {}^7F_2$ (613.2, 617.4), $^5D_0 \rightarrow {}^7F_3$ (652 and 655 nm), and $^5D_0 \rightarrow {}^7F_4$ (692.4 and 703.4 nm). The transition $^5D_0 \rightarrow {}^7F_0$ presents only one line, which is consistent with only one site being occupied by the Eu^{3+} ion. Since there are only a few fine structures observed in the $^5D_0 \rightarrow {}^7F_{1-4}$ transitions of Eu(TTA-Si)$_3$, no information can be found on the Eu^{3+} site symmetry. However, the shape of the emission spectrum, i.e., the ratios of integrated emission intensities $I(^5D_0 \rightarrow {}^7F_{J=0,2-6})$ to $I(^5D_0 \rightarrow {}^7F_1)$ may be used to calculate the radiative rate, the $A_{rad} = \Sigma A_{0-J}$ and the Ω_2 and Ω_4 Judd−Ofelt intensity parameters, which give indications about the average local field at the europium ion. Details of the calculation have been given by Werts and co-workers.[31] In that paper it has been shown that the values of the Judd−Ofelt parameters extracted from the Eu^{3+} emission spectra are in reasonable agreement with those determined from absorption data. Actually, calculation from the emission spectrum has proven to be very convenient for comparing different kinds of compounds containing Eu^{3+}, especially when absorption data are not available, and have been used very often as shown in review articles.[5,6] Care must be taken to perform measurements with the same experimental details and to correct emission spectra for the instrumental response versus wavelength, as it has been done here in order to compare the neat complex and the hybrids. The radiative rate of a $^5D_0 \rightarrow {}^7F_J$ transition may be written as in eq 1

$$A_{0-J} = \frac{64\pi^4\tilde{\nu}^3}{3h(2J+1)}\left[\frac{n(n^2+2)^2}{9}D_{ED} + n^3 D_{MD}\right] \qquad (1)$$

where $\tilde{\nu}$ is the average transition energy in cm^{-1}, h the Planck constant, and n the medium's refractive index, and D_{ED} and D_{MD} are the electric and magnetic dipole strengths, respectively. The $^5D_0 \rightarrow {}^7F_1$ emission is purely magnetic dipolar and its radiative rate does not depend on the local field imposed by the environment; its oscillator strength has been calculated by theory, $D_{MD} = 9.6 \times 10^{-42}$ esu^2 cm^2, giving from eq 1, $A_{0-1} = 14.65n^3$ in s^{-1}. The experimental $I(^5D_0 \rightarrow {}^7F_J)$, i.e., the integrated area of the emission transition, is directly proportional to the corresponding radiative rate A_{0-J}, to the number of active ions in the emitting volume, and to a number of instrumental parameters hard to estimate, but this difficulty is overcome by considering the intensities relative to $I(^5D_0 \rightarrow {}^7F_1)$, taken as a reference. The A_{0-J} in s^{-1} may be calculated with $I(^5D_0 \rightarrow {}^7F_J)/I(^5D_0 \rightarrow {}^7F_1) = A_{0-J}/A_{0-1} = A_{0-J}/14.65n^3$. The $A_{rad} = \Sigma A_{0-J}$ and $\tau_{rad} = 1/A_{rad}$ are given in Table 1, calculated with an average value $n = 1.5$ and with the usually admitted approximation that $^5D_0 \rightarrow {}^7F_{5,6}$ have negligible intensities. The transitions $^5D_0 \rightarrow {}^7F_{2,4,6}$ are purely electric dipolar and, according to the Judd−Ofelt theory, their

Table 1. Judd−Ofelt Intensity Parameters (Ω_2, Ω_4), Radiative Rates (A_{rad}), Radiative and Experimental Lifetimes (τ_{rad}, τ_{exp}), and Quantum Efficiencies (q)[a]

	Ω_2 ($\times 10^{-20}$ cm^2)	Ω_4 ($\times 10^{-20}$ cm^2)	A_{rad} (ms^{-1})	τ_{rad} (ms)	τ_{exp} (ms)	q	n_{OH}	n_w
$Eu(TTA)_3(H_2O)_2$[28]	33	4.6	0.79	1.26	0.26	0.21	5.5	3.0
$Eu(TTA\text{-}Si)_3$	40 ± 2	5.9 ± 0.3	1.15 ± 0.06	0.87 ± 0.04	0.56 ± 0.06	0.64 ± 0.06	0	0.4
SiO_2-*meso*-$Eu(TTA\text{-}Si)_3$	13.5 ± 0.7	4.3 ± 0.2	0.82 ± 0.04	1.22 ± 0.06	0.26 ± 0.03	0.21 ± 0.02	5.4	3.0
SiO_2- $Eu(TTA\text{-}Si)_3$	13.8 ± 0.7	5.8 ± 0.3	0.66 ± 0.03	1.52 ± 0.08	0.14 ± 0.01	0.09 ± 0.01	13.3	6.9
SiO_2@$Eu(TTA\text{-}Si)_3$	9.0 ± 0.4	6.2 ± 0.3	0.45 ± 0.02	2.2 ± 0.1	0.43 ± 0.04	0.19 ± 0.02	2.8	1.7

[a] n_{OH}, n_w: number of equivalent OH and water molecules estimated following eq 5 or eq 6 (see text).

oscillator strengths are expressed following eq 2 in esu^2 cm^2 with e the elementary charge.

$$D_{ED} = e^2 \sum_{\lambda=2,4,6} \Omega\lambda |\langle J || U^{(\lambda)} || J' \rangle|^2 \quad (2)$$

The reduced matrix elements are zero, except $|\langle 0||U^{(2)}||2\rangle^2|$ and $|\langle 0||U^{(4)}||4\rangle^2| = 0.0023$. The values of A_{0-2} and A_{0-4} are thus related directly with the Judd−Ofelt intensity parameters Ω_2 and Ω_4, respectively. For $Eu(TTA\text{-}Si)_3$, $\Omega_2 = 40 \times 10^{-20}$ cm^2 and $\Omega_4 = 5.9 \times 10^{-20}$ cm^2 could be compared with the values $\Omega_2 = 33 \times 10^{-20}$ cm^2 and $\Omega_4 = 4.6 \times 10^{-20}$ cm^2 obtained for the related complex $Eu(TTA)_3(H_2O)_2$.[28] The high value found for Ω_2 traduces the high intensity of the hypersensitive transition $^5D_0 \rightarrow {}^7F_2$ and means that the site occupied by the Eu^{3+} ion is not centrosymmetrical and that the ligand field is strongly polarizing. The other value of interest is the $^5D_0$ radiative lifetime τ_{rad}. By comparing the observed lifetime (τ_{exp}) with the radiative one, the $^5D_0$ emission quantum efficiency ($q = \tau_{exp}/\tau_{rad}$) is calculated. The luminescence decay curve, with emission monitored at $^5D_0 \rightarrow {}^7F_2$, could be fitted by a monoexponential decay function and the lifetime value (τ_{exp}) so obtained was 0.56 ± 0.06 ms. The radiative lifetime was $\tau_{rad} = 0.87 \pm 0.04$ ms, and the emission quantum efficiency was therefore $q = 0.64 \pm 0.06$. This value is considerably higher than the one found for the $Eu(TTA)_3(H_2O)_2$ complex ($q = 0.21 \pm 0.02$) which may be assigned due to the absence of water molecules coordinated to Eu^{3+} in $Eu(TTA\text{-}Si)_3$. We proposed that the coordination sphere of the europium is here stabilized by intramolecular interactions of the nearby methoxy functions of the pending group of the TTA-Si ligand.

The emission of $Eu(TTA\text{-}Si)_3$ in solution (Figure 2) is also governed by $^5D_0 \rightarrow {}^7F_2$ observed with maximum at 611.6 nm, slightly broadened compared with the solid state spectrum. Experimental and radiative lifetime values in solution were 0.60 ± 0.06 and 1.33 ± 0.07 ms and therefore the quantum efficiency value is $q = 0.45 \pm 0.05$. The difference in the τ_{rad} values obtained for the solid complex and its solution means existence of supplementary intermolecular interactions of solvent molecules with the emitting center.

The quantum yield (ϕ) is the ratio of emitted to absorbed photons. It is a current practice to obtain the relative quantum yield (ϕ') by using well-known species as references. In this work ϕ' was obtained for the acetonitrile−Eu^{3+} complex solution by using the complex $[Ru(bipy)_3]Cl_2$ as a reference (ϕ = 2.8% in water, λ_{exc}= 400 nm)[32] (eq 3)

$$\phi = \left(\frac{Abs_R}{Abs_X}\right)\left(\frac{Em_X}{Em_R}\right)\left(\frac{n_X}{n_R}\right)^2 \phi_R \quad (3)$$

where Abs is the absorbance at the excitation wavelength, Em is emission intensity, and n is the refractive index of the solvent used. Subscripts R and X refer to the reference and the unknown, respectively. By doing that with the absorbance value measured at the excitation wavelength (365 nm) and the emission intensity taken as the integrated emission spectra from 400 to 710 nm, the value $\phi' = 0.30$ is obtained which should be compared with the q value of 0.45 ± 0.05, since the q value expresses the maximum possible value for ϕ'. The ratio ϕ'/q should express the efficiency of the energy transfer which in this case amounts to 66%.

3.2. $Eu(TTA\text{-}Si)_3$-Functionalized Silica-Based Nanohybrids. The silylated europium complex is an elegant approach to bring an intense red luminescence at the silica nanoparticles. This methodology allows free design of the substrate, as dense or porous, as micro- or nanosized, and subsequently, makes possible the one-step covalent bonding of the luminescent complex hindering the leaching process. Following the methodology chosen, silylated europium complex covalently incorporated on the bulk of silica (Scheme 1c) or grafted at the silica surface (Scheme 1d) could be obtained. Further reactions of such functionalized silica-based material may be carried out without complex release.

Grafting reactions were undertaken by reacting an excess of complex with the silica matrix at room temperature. When mesoporous silica matrix was used as starting silica, substrate activation by heating under vacuum ascertains the absence of physisorbed molecules such as water or residual directing agent and the reaction involves dry ethanol. Whereas for the grafting of $Eu(TTA\text{-}Si)_3$ on Ludox silica the presence of water cannot be prevented, we minimized it to the amount of the Ludox sol. In both cases, silica particles are purified by dialysis and further washings and centrifugations.

If incorporation of inorganic luminophor, such as tris-(dipyridine)ruthenium(II) complex, $[Ru(bpy)_3]^{2+}$, is largely reported in the literature,[33−35] very few examples of europium complex have been incorporated in silica nanoparticles using a Stober-type reaction. Synthesis of well spherical nanoparticles uniform in size needs scrupulous experimental conditions closely related to the protocol proposed by Tan et al.[33,34] Modification of the luminescent complex required modification of this protocol, and Yuan et al.[36] synthesized 42 ± 3 nm silica particles incorporating unsilylated terbium(III) complex using a mixture of two quaternary reverse microemulsions based on Triton X-100, hexanol, cyclohexane, and water. As mentioned in the Introduction, Li et al.[23] succeeded in obtaining 40 ± 5 nm silica particles incorporating silylated europium complex using Tan's protocol varying the water to surfactant ratio from 10 to 6.7. In this case, the cosurfactant to surfactant ratio remains equal to 5. Numbers of experimental conditions have been evaluated to incorporate $Eu(TTA\text{-}Si)_3$. Optimization of the one-step incorporation reaction required the evaluation of a lot of parameters such as temperature, ammonia concentration, chemical nature of

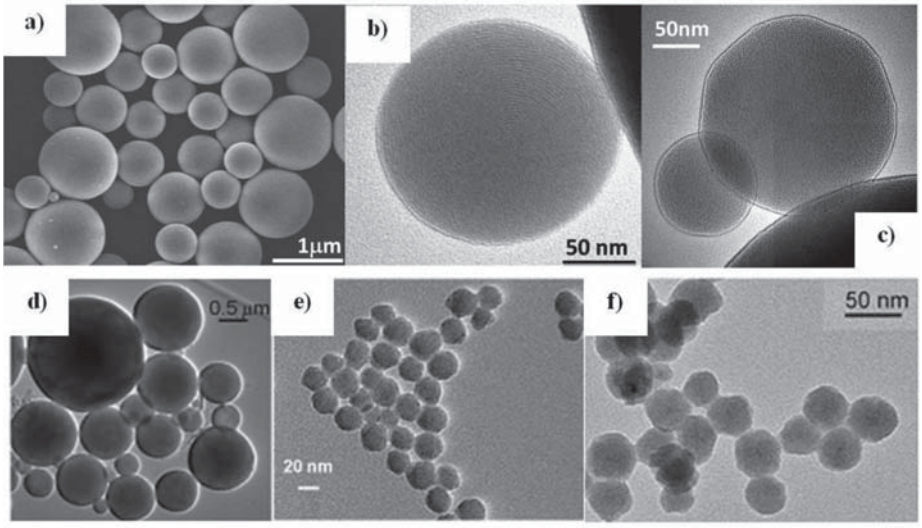

Figure 4. Electron microscopy images of starting mesoporous particles (SEM, a; TEM, b,c) and TEM images of different hybrids SiO_2-*meso*-Eu(TTA-Si)$_3$ (d); SiO_2-Eu(TTA-Si)$_3$ (e); and SiO_2@Eu(TTA-Si)$_3$ (f).

the surfactant (Triton X-100, AOT), and cosurfactant (hexanol, octanol). All these parameters influenced the quality and the size of the silica nanoparticles obtained. The quaternary system reported did not allow us to obtain convenient nanoparticles perhaps due to the different solubility of the starting europium complex, and the affinity of the europium toward oxygen atoms of surfactant and cosurfactant molecules. Optimized conditions were found changing hexanol to octanol as cosurfactant and slightly decreasing the cosurfactant to surfactant molar ratio from 5 to 4.1. In these conditions, SiO_2@Eu(TTA-Si)$_3$ as well spherical silica nanoparticles, uniform in size, incorporating Eu(TTA-Si)$_3$ was isolated.

Figure 4 shows EM images of starting mesoporous particles (a, b, c) and of the three silica-based materials SiO_2-*meso*-Eu(TTA-Si)$_3$ (d), SiO_2-Eu(TTA-Si)$_3$ (e), and SiO_2@Eu(TTA-Si)$_3$ (f). The mesoporous silicas obtained with the spray−pyrolysis method are spherical submicronic particles with a relatively important size dispersion (600 ± 300 nm) (Figure 4a). The mesochannels in each sphere form very well ordered hexagonal arrays with a pore diameter of about 2.2 nm (Figure 4b,c). The interest of such silica particles is their large surface area (940 m^2/g) that promotes high level of grafting, providing free diffusion inside the pores. Grafting at the external surface of the particles is also possible but remains a minor situation because the external surface of 600 nm particles is estimated to be no more than 10% of its total surface. A characteristic TEM image of the grafted particles SiO_2-*meso*-Eu(TTA-Si)$_3$ is given Figure 4d showing that the size and external morphology were retained. However, the porous system was not evident after grafting probably because the silylated complex provides minor electronic density difference with the silica matrix. As expected, the SiO_2-Eu(TTA-Si)$_3$ (Figure 4e) appear with an uniform size (28 ± 3 nm) slightly increased from the size of the commercial starting particles (24 ± 2 nm). Dense silica particles SiO_2@Eu(TTA-Si)$_3$ obtained by the modified Stober reaction are well spherical and also uniform in size of 40 ± 2 nm (Figure 4f). Because silylated europium complex was hydrolyzed and aggregated in the water pool in the microemulsion together with the silica network being formed, europium complex is expected to be embedded into the particle.

DRIFT spectra show the signature of the silylated europium complex in each silica material with the presence of the stretching vibration of the ketone group at 1630 cm^{-1} together with a fine band at 1414 cm^{-1} of the thienyl moiety. The most important change is observed in the 1200−1000 cm^{-1} range where the signature of the complex ($\upsilon(CF_3)$, $\upsilon(Si-C)$) is overlaid with the characteristics of the siloxane bulk ($\upsilon(Si-C)$, $\upsilon(Si-O)$, $\delta(Si-O-C)$) involving a slight shift and increase of the maxima at 1230 cm^{-1}. Moreover, the spectrum of europium-incorporated nanohybrid, SiO_2@Eu(TTA-Si)$_3$, exhibits weak bands at 2980 and 2878 cm^{-1} corresponding to asymmetric and symmetric stretching vibrations of alkyl groups, respectively.

Table 2 gives grafting and incorporation ratios, *R*, expressed in millimoles of complex per gram of silica. These values are calculated from elemental analysis based on the sulfur content. Values are in the range 0.41−0.12 mmol/g. The grafting ratio observed for the mesoporous material (0.41 mmol/g) is significantly higher than the europium loading reported for MCM-41 materials of about 2.0 wt % (0.13 mmol/g).[20] The grafting ratio observed on Ludox silica (0.21 mmol/g) agrees well with our previous work. The number of grafted complexes per nm^2 can be calculated using the observed grafting ratios and the specific areas of starting materials. Around 1 europium complex per nm^2 is grafted on Ludox whereas 0.29 complex per nm^2 is grafted on mesoporous material. This difference can be attributed to the different hydroxylation ratios of each silica matrix since amount of free silanol groups available for grafting is lower for freshly activated mesoporous silica than for Ludox silica aqueous sol. Successful microemulsion process allows incorporation of an interesting amount of Eu(TTA-Si)$_3$ since according to the sulfur content an amount of 0.12 mmol of complex per gram of silica has been calculated. This value is in agreement and slightly higher than that observed by Yuan et al.[36] when Tb(BPTA) is incorporated. In this last case, they evaluated the incorporation ratio at ∼1500 complexes per nanoparticle of 42 nm diameter which can be traduced by 0.034 mmol of complex per gram of silica. In our conditions, the presence of the silyl group induces the efficient confinement of the complex to the silica network.

Table 2. Size Distribution and Complex Grafting or Incorporation Ratios (R) for the Three Types of Hybrids

$Eu(TTA\text{-}Si)_3$ functionalized hybrids	av size (nm)	R (mmol of $Eu(TTA\text{-}Si)_3$/ g silica)	$N(Eu(TTA\text{-}Si)_3)$/ nm^2
SiO_2-*meso*-$Eu(TTA\text{-}Si)_3$	600 ± 300	0.41	0.29
SiO_2-$Eu(TTA\text{-}Si)_3$	28 ± 3	0.21	0.90
SiO_2@$Eu(TTA\text{-}Si)_3$	40 ± 5	0.12	–

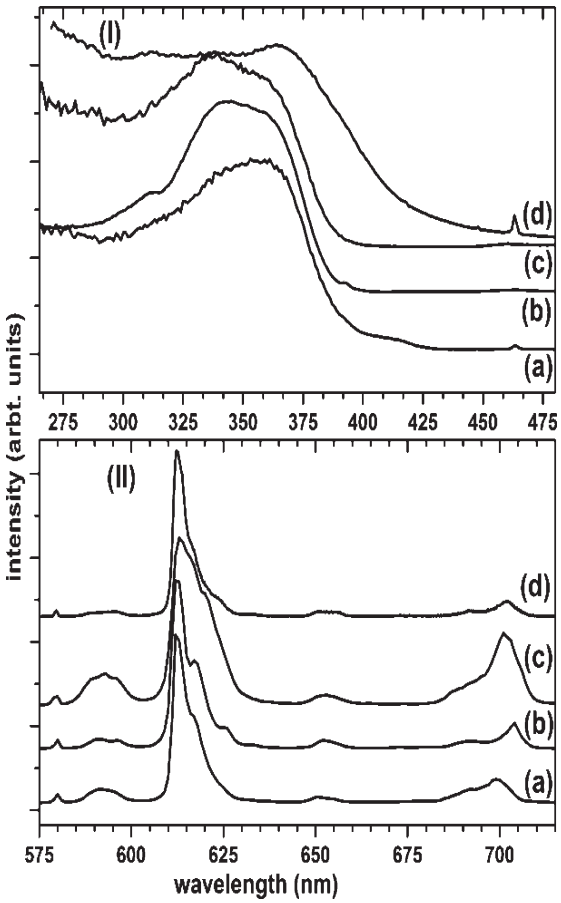

Figure 5. Luminescence results for modified silica particles. (I) Excitation spectra ($\lambda_{emission}$ at 612 nm) and (II) emission spectra ($\lambda_{excitation}$ at 365 nm) for the different solid samples, at 298 K: (a) SiO_2-$Eu(TTA\text{-}Si)_3$, (b) SiO_2-*meso*-$Eu(TTA\text{-}Si)_3$, (c) SiO_2@$Eu(TTA\text{-}Si)_3$, and (d) $Eu(TTA\text{-}Si)_3$.

Figure 5 shows excitation and emission luminescence spectra obtained for each hybrid and also those of the $Eu(TTA\text{-}Si)_3$ free complex. About excitation, the same bands already seen for the pure complex are observed for the hybrid systems (Figure 5 (I)). The ligand to europium antenna effect is observed below 400 nm as broad near-UV bands, the Eu^{3+} 4f−4f transitions being very weak in the visible region. In the pure powdered compound $Eu(TTA\text{-}Si)_3$, the high absorption cross section of light in the near-UV (<370 nm) leads to a saturation of the monitored emission, which results in distortions of the excitation spectrum, an artifact already reported and discussed by Blasse and coworkers.[37] At the three hybrids, however, this concentration effect is not seen and the saturation is no longer observed, so that the shapes of the excitation spectra may be compared and are actually very similar showing an efficient antenna effect.

Figure 5(II) shows emission spectra from which Ω_2, Ω_4, and A_{rad} were calculated and are given in Table 1. The spectra recorded for SiO_2-$Eu(TTA\text{-}Si)_3$ and for SiO_2-*meso*-$Eu(TTA\text{-}Si)_3$ (Figure 5, IIa and IIb) are rather similar, which is traduced by the fact that their respective Ω_2 and Ω_4 are comparable. For the third nanohybrid, SiO_2@$Eu(TTA\text{-}Si)_3$, a broadening is observed (Figure 5(IIc)), and the overall shape of the spectrum is completely different from the others, as it is traduced in particular by the weak value of Ω_2. A decrease in the Ω_2 parameter is observed for all particles in comparison with the pure $Eu(TTA\text{-}Si)_3$. Since this parameter gives the overall contribution of symmetry effects together with the ligand field polarization, it can be said that a weaker ligand field is observed by Eu^{3+}, leading to lower radiative rates A_{rad}. Important decreases are also observed for experimental lifetimes. For the hybrids, luminescence decay curves were nonexponential, and for that an average value for τ_{exp} was obtained by using the expression (eq 4).

$$\tau_{exp} = \frac{\int_0^\infty I(t)t\ dt}{\int_0^\infty I(t)\ dt} \tag{4}$$

For the pure complex, the nonradiative decay probability, $1/(\tau_{N\text{-}rad}) = 1/(\tau_{exp}) - 1/(\tau_{rad}) = 1/(\tau_{diketones}) = 0.636\ ms^{-1}$, is essentially due to the coupling of $^5D_0$ electronic level with the vibrations of the three diketonate groups. The additional nonradiative de-excitation pathways in the nanohybrids are more probably due to the coupling with the high energy vibrations of hydroxyl groups. We thus employ the formula (eq 5) to evaluate n_{OH}, the number of equivalent OH vibrators linked to Eu.

$$n_{OH} = \frac{1}{0.44}\left(\frac{1}{\tau_{exp}} - \frac{1}{\tau_{rad}} - 0.636\right) \tag{5}$$

In this equation, 0.44 ms^{-1} is the rate of $^5D_0$ de-excitation by coupling with one OH. It has been proposed by Supkowski and Horrocks[38] for alcohol OH, and is similar to the one which was deduced from determinations performed in highly hydrated inorganic matrices;[39] this value was taken here to calculate the n_{OH} gathered in Table 1.

The equivalent number of OH oscillators may also be estimated as twice n_w, the number of water molecules at the Eu^{3+} first coordination shell, calculated with the formula (eq 6).

$$n_w = 1.11\left(\frac{1}{\tau_{exp}} - \frac{1}{\tau_{rad}} - 0.31\right) \tag{6}$$

This equation was employed in the literature in order to have approximate results for solid-state studies;[40] it was taken by analogy with the Horrocks formula.[38] The numbers of equivalent OH oscillators calculated by each of the two methods (n_{OH} and $2n_W$ in Table 1) are in reasonable agreement, and the average value will be considered to compare the nanohybrids with one another.

For SiO_2-*meso*-$Eu(TTA\text{-}Si)_3$, 5.7 OH were found, nearly the 5.75 OH calculated for $Eu(TTA)_3(H_2O)_2$. The approximations made for the calculations lead to the overestimation of the number of hydroxyls since there are only 4 OH linked to

europium in the last compound. We may nevertheless retain that $Eu(TTA\text{-}Si)_3$ molecules have been grafted at the surface of the silica walls, keeping the structure with three diketonates groups chelating Eu^{3+}. Some hydroxylated molecules are also bound to europium, either ethanol from the reaction medium or methanol produced by the reaction. When the complex was grafted at the surface of AS40 dense silica particles, the calculated number of equivalent OH oscillators (13.5) was very high. Although the numbers of equivalent OH oscillators are always overestimated, they may nevertheless be compared and it may be concluded that there are noticeably more OH linked to Eu^{3+} in SiO_2-$Eu(TTA\text{-}Si)_3$ than in SiO_2-*meso*-$Eu(TTA\text{-}Si)_3$. This is well in line with the reaction procedure starting from an aqueous sol of silica nanoparticles. This residual water may coordinate the Eu^{3+} and it has also the effect to hydrolyze the nongrafted methoxy groups of the complex. The length of the propyl chain allows an intramolecular interaction between these terminal silanols and the cation, increasing finally the number of hydroxyls able to quench the $^5D_0$ emission of Eu^{3+}.

In W/O microemulsion, the europium complex is hydrolyzed together with the TEOS in order to create the siloxane network. This induces deformations of the coordination sphere of the europium center which is demonstrated by the broad emission lines (Figure 5c) like in a glass. In this case, europium ions are stabilized by nearby oxygen atoms of the siloxane network in agreement with the low value of the quenching hydroxyl groups (n_{OH} = 3.2) compared to the grafted nanohybrids.

Finally, it is important to compare the radiative rates, A_{rad}, and the luminescence efficiencies, q (Table 1) considering also characteristics required for possible applications as biolabels. The $Eu(TTA\text{-}Si)_3$-grafted mesoporous particles have a high radiative rate associated with a good efficiency (A_{rad} = 0.82 ± 0.04 ms^{-1}, q = 0.21 ± 0.02) in comparison with the values for organic−inorganic hybrids containing Eu^{3+} which have been gathered in Table 3 in the review.[5] The essential drawback of these particles is their large size dispersion (600 ± 300 nm). Efforts are in progress to synthesize mesoporous luminescent particles with better size control which could be considered as platforms for bioanalysis applications. Whereas SiO_2-$Eu(TTA\text{-}Si)_3$ nanoparticles are very well monodispersed (28 ± 3 nm), their radiative rate is lower than for mesoporous substrate (A_{rad} = 0.66 ± 0.03 ms^{-1}) and furthermore, their quantum efficiency is rather low (q = 0.09 ± 0.01) because of the presence of a number of hydroxyl groups quenching the $^5D_0$ emission. Silica nanoparticles incorporating the $Eu(TTA\text{-}Si)_3$ complex are uniform in size (40 ± 5 nm). They display a radiative rate (A_{rad} = 0.45 ± 0.02 ms^{-1}) in the average of the reported values,[6] associated with a good quantum efficiency (q = 0.19 ± 0.02). These nanohybrids are good candidates for luminescent labeling within living cells since further reactivity such as chemical functionalization can then be planned on their hydroxylated surface.

4. CONCLUSION

We developed an original strategy with a view to obtain luminescent silica-based hybrids containing europium chelates. In this way, we have synthesized a new monosilylated TTA derivative which is both a good chelating ligand and an excellent antenna for Eu^{3+} emission. Moreover, interest of this ligand lies in the presence of alkoxysilyl groups, bonded to the TTA molecule by α-carbon alkylation reaction, for covalent bonding to silica materials. The europium complex $Eu(TTA\text{-}Si)_3$ was fully characterized by elemental analysis, mass spectrometry, FTIR, and electronic spectroscopy. The formula proposed was $Eu(TTA\text{-}Si)_3$ where three diketonato ligands are coordinated to the europium ion which coordination sphere is completed by supplementary intramolecular interactions of some methoxysilyl groups.

Judd−Ofelt $\Omega_{2,4}$ intensity parameters and radiative and nonradiative decay rates for the Eu^{3+} $^5D_0$ excited state were evaluated. The value obtained for the Ω_2 (40×10^{-20} cm^2) was observed to be higher than the value obtained for the related $Eu(TTA)_3(H_2O)_2$ well-known from the literature, suggesting a stronger polarizing effect for Eu^{3+} ligand field. The emission quantum efficiency was 0.64 ± 0.06 for $Eu(TTA\text{-}Si)_3$, a high value that could be compared with the value of 0.21 known for $Eu(TTA)_3(H_2O)_2$.

The new $Eu(TTA\text{-}Si)_3$ complex has been covalently bonded to three different silica particles: commercial silica nanoparticles (Ludox AS40), mesoporous silica particles prepared by spray pyrolysis methodology, and silica particles prepared from TEOS. Regardless of their size dispersity, spray pyrolysis synthesized mesoporous silica particles appeared to be a more interesting matrix for luminescence intensity than Ludox silica nanoparticles (quantum efficiencies q = 0.21 ± 0.02 and 0.09 ± 0.01, respectively). Novel nanoparticles (40 ± 5 nm in size) incorporating $Eu(TTA\text{-}Si)_3$ in silica were obtained using a water in oil reverse microemulsion procedure taking benefit of the networking function of the silylated europium complex. These NPs exhibit strong antenna effect and their quantum efficiency is q = 0.19 ± 0.02. Such luminescent particles could be used in applications where stability of silica particles and high emission intensity are required simultaneously. Our results emphasize a promising strategy using a silylated europium(III) complex to obtain functionalized silica nanoparticles for the engineering of new luminescent biolabels. More generally, the utilization of a silylated ligand has to be considered for direct grafting of the Eu^{3+} luminescent complex on any silica surface previously prepared.

AUTHOR INFORMATION

Corresponding Author

*E-mail: menu@chimie.ups-tlse.fr. Tel: +33 5 61 55 84 87. Fax: +33 5 61 55 61 63.

ACKNOWLEDGMENT

The authors thank the Brazilian agencies FAPESP, CNPq, CAPES, and CAPES-COFECUB Brazil-France cooperation program for the grant to A.P.D.

REFERENCES

(1) Richardson, F. S. *Chem. Rev.* **1982**, *82*, 541–552.
(2) Escribano, P.; Julian-Lopez, B.; Planelles-Arago, J.; Cordoncillo, E.; Viana, B.; Sanchez, C. *J. Mater. Chem.* **2008**, *18*, 23–40.
(3) Eliseeva, S. V.; Bunzli, J.-C. G. *Chem. Soc. Rev.* **2010**, *39*, 189–227.
(4) Buenzli, J.-C. G.; Piguet, C. *Chem. Soc. Rev.* **2005**, *34*, 1048–1077.
(5) Carlos, L. D.; Ferreira, R. A. S.; Bermudez, V. D.; Ribeiro, S. J. L. *Adv. Mater.* **2009**, *21* (5), 509–534.
(6) Binnemans, K. *Chem. Rev.* **2009**, *109*, 4283–4374.
(7) Zhang, C.; Sun, L.; Zhang, Y.; Yan, C. *J. Rare Earths* **2010**, *28*, 807–819.
(8) Huhtinen, P.; Kivelae, M.; Kuronen, O.; Hagren, V.; Takalo, H.; Tenhu, H.; Loevgren, T.; Haermae, H. *Anal. Chem.* **2005**, *77*, 2643–2648.

(9) Li, H. R.; Lin, J.; Zhang, H. J.; Fu, L. S.; Meng, Q. G.; Wang, S. B. *Chem. Mater.* **2002**, *14*, 3651–3655.
(10) Binnemans, K.; Lenaerts, P.; Driesen, K.; Goerller-Walrand, C. *J. Mater. Chem.* **2004**, *14*, 191–195.
(11) Wang, X.-L.; Yan, B.; Liu, J.-L. *Photochem. Photobiol. Sci.* **2011**, *10*, 580–586.
(12) Li, H. R.; Yu, J. B.; Liu, F. Y.; Zhang, H. J.; Fu, L. S.; Meng, Q. G.; Peng, C. Y.; Lin, J. *New J. Chem.* **2004**, *28* (9), 1137–1141.
(13) Lenaerts, P.; Goerller-Walrand, C.; Binnemans, K. *J. Lumin.* **2006**, *117*, 163–169.
(14) Lenaerts, P.; Storms, A.; Mullens, J.; D'Haen, J.; Goerller-Walrand, C.; Binnemans, K.; Driesen, K. *Chem. Mater.* **2005**, *17*, 5194–5201.
(15) Meng, Q.; Boutinaud, P.; Zhang, H.; Mahiou, R. *J. Lumin.* **2007**, *124*, 15–22.
(16) Cides, d. S. L. C.; Martins, T. S.; Santos, F. M.; Teotonio, E. E. S.; Isolani, P. C.; Brito, H. F.; Tabacniks, M. H.; Fantini, M. C. A.; Matos, J. R. *Microporous Mesoporous Mater.* **2006**, *92*, 94–100.
(17) DeOliveira, E.; Neri, C. R.; Serra, O. A.; Prado, A. G. S. *Chem. Mater.* **2007**, *19*, 5437–5442.
(18) Yan, B.; Zhou, B. *J. Photochem. Photobiol., A* **2008**, *195* (2−3), 314–322.
(19) Li, Y.; Yan, B.; Yang, H. *J. Phys. Chem. C* **2008**, *112*, 3959–3968.
(20) Gago, S.; Fernandes, J. A.; Rainho, J. P.; Ferreira, R. A. S.; Pillinger, M.; Valente, A. A.; Santos, T. M.; Carlos, L. D.; Ribeiro-Claro, P. J. A.; Goncalves, I. S. *Chem. Mater.* **2005**, *17*, 5077–5084.
(21) Charbonniere, L. J.; Weibel, N.; Estournes, C.; Leuvrey, C.; Ziessel, R. *New J. Chem.* **2004**, *28* (7), 777–781.
(22) Gulino, A.; Lupo, F.; Condorelli, G. G.; Motta, A.; Fragala, I. L. *J. Mater. Chem.* **2009**, *19*, 3507–3511.
(23) Zhang, H.; Xu, Y.; Yang, W.; Li, Q. *Chem. Mater.* **2007**, *19*, 5875–5881.
(24) Cousinie, S.; Gressier, M.; Reber, C.; Dexpert-Ghys, J.; Me nu, M.-J. *Langmuir* **2008**, *24*, 6208–6214.
(25) Cousinie, S.; Gressier, M.; Alphonse, P.; Menu, M.-J. *Chem. Mater.* **2007**, *19*, 6492–6503.
(26) Qiao, X. F.; Yan, B. *J. Phys. Chem. B* **2009**, *113*, 11865–11875.
(27) Rocha, L. A.; Caiut, J. M. A.; Messaddeq, Y.; Ribeiro, S. J. L.; Martines, M. A. U.; Freiria, J. d. C.; Dexpert-Ghys, J.; Verelst, M. *Nanotechnology* **2010**, *21*, 155603/6.
(28) Malta, O. L.; Brito, H. F.; Menezes, J. F. S.; Goncalves e Silva, F. R.; Alves, S., Jr.; Farias, F. S., Jr.; de Andrade, A. V. M. *J. Lumin.* **1997**, No. 75, 255–268.
(29) Teotinio, E. S. E.; Fett, G. M.; Brito, H. F.; Faustino, W. M.; de Sa, G. F.; Felinto, M. C. F. C.; Santos, R. H. A. *J. Lumin.* **2008**, *128*, 190–198.
(30) Lamansky, S.; Djurovich, P.; Murphy, D.; Abdel-Razzaq, F.; Lee, H.-E.; Adachi, C.; Burrows, P. E.; Forrest, S. R.; Thompson, M. E. *J. Am. Chem. Soc.* **2001**, *123*, 4304–4312.
(31) Werts, M. H. V.; Jukes, R. T. F.; Verhoeven, J. W. *Phys. Chem. Chem. Phys.* **2002**, *4*, 1542–1548.
(32) Nakamura, S.; Takei, S.; Akiba, K. *Anal. Sci.* **2002**, *18*, 319–323.
(33) Wang, L.; Wang, K. M.; Santra, S.; Zhao, X. J.; Hilliard, L. R.; Smith, J. E.; Wu, J. R.; Tan, W. H. *Anal. Chem.* **2006**, *78*, 646–654.
(34) Santra, S.; Zhang, P.; Wang, K.; Tapec, R.; Tan, W. *Anal. Chem.* **2001**, *73*, 4988–4993.
(35) Bagwe, P. R.; Yang, C.; Hilliard, L. R.; Tan, W. *Langmuir* **2004**, *20*, 8336–8342.
(36) Ye, Z.; Tan, M.; Wang, G.; Yuan, J. *Anal. Chem.* **2004**, *76*, 513–518.
(37) Blasse, G.; Meijerink, A.; de Mello Donega, C *J. Alloys Compd.* **1995**, *225*, 24–27.
(38) Supkowski, R. M.; Horrocks, W. D., Jr. *Inorg. Chim. Acta* **2002**, *340*, 44–48.
(39) Caiut, J. M. A.; Ribeiro, S. J. L.; Messaddeq, Y.; Dexpert-Ghys, J.; Verelst, M.; Dexpert, H. *Nanotechnology* **2007**, *18* (45), 455605.
(40) Dias, F. A.; Carlos, L. D.; Messadeq, Y.; Ribeiro, S. J. L. *Langmuir* **2005**, *21*, 1776–1783.